

## Research paper

## Advancements in wideband source localization with an acoustic vector sensor line array



Bowen Dong, Haifeng Zhang\*, Shengtian Sang, Yan Zhang

MEMS Center, Harbin Institute of Technology, Harbin, Heilongjiang, 150001, China

## ARTICLE INFO

## Keywords:

Wideband acoustic source localization  
Acoustic vector sensors  
Coherent processing

## ABSTRACT

A method is presented for localizing wideband acoustic sources using an array of acoustic vector sensors (AVS). The method focuses on leveraging the lack of correlation between acoustic pressure and particle velocity in the underwater environmental noise field. Coherent processing is introduced in the signal processing stage to suppress noise components in the observed data. By employing a focused transform that maps various frequency components of the wideband signal into the same signal subspace, an asymptotically unbiased Direction of Arrival (DOA) estimation is achieved using a multidimensional subspace method. A concise expression for the Cramér-Rao Bound (CRB) on the estimation errors is provided within the framework of the wideband multi-vector-sensor model. The performance of the proposed method for localizing sources is assessed through simulation and experimental data analysis. The research indicates that coherent processing effectively suppresses isotropic components in background noise, the proposed method achieves a lower estimation error, closer to the CRB, compared to the scalar array counterpart under identical signal-to-noise ratio (SNR) conditions.

## 1. Introduction

The accurate estimation of the Direction of Arrival (DOA) for underwater acoustic sources is of paramount importance in various applications, including navigation, communication, and surveillance in marine environments. Common approaches for DOA estimation include beamforming and subspace methods. Subspace methods, such as Multiple Signal Classification (MUSIC) and Subspace Fitting (SF), offer high angular resolution and localization accuracy, making them well-suited for narrowband source localization.

Nevertheless, underwater acoustic sources often exhibit wideband and coherent properties, presenting both challenges and opportunities for localization techniques (D.A. Abraham, 2019). One approach to addressing wideband coherent signals is frequency-domain Discrete Fourier Transform (DFT) beamforming (Chen, J. C. et al., 2003), which employs rectangular window filtering in the frequency domain. This method may lead to discontinuities in the output time series segments. Wideband focusing algorithms offer advantages in handling wideband coherent source localization with low computational requirements (Jiang M. et al., 2023), achieved by mapping observations from different frequency points to a common reference frequency using a focusing matrix. Subsequently, subspace methods can be employed to estimate

the DOA.

Prominent wideband focusing algorithms include the coherent signal-subspace method (CSS) and two-sided transformation (TCT). The CSS method is plagued by an asymptotic bias in peak estimation, attributed to the reliance on azimuthal prior-estimation for constructing the focusing matrix. Moreover, uncertainty in the short-time spectrum can lead to spatial spectral instability, introducing errors in azimuth estimation (Wang H. and Kaveh M., 1985). In contrast, the introduction of the two-sided transformation (TCT) mitigates focusing errors. The TCT algorithm has been shown to provide unbiased estimates for wideband source localization, offering significant advantages over CSS (Valaee and Kabal, 1995).

The emergence of acoustic vector sensors (AVS) has revolutionized the landscape of underwater acoustic signal processing, providing novel insights into the detection and parameter estimation of wideband signals. These sensors offer a new paradigm by providing a joint measurement of acoustic pressure and particle velocity. This simultaneous acquisition captures rich information embedded in underwater signals, expanding the post-signal processing domain.

The study by Huawei Chen and Junwei Zhao (Chen and Zhao, 2005) extends the concept of wideband focusing to the processing of AVS. It validates that AVS arrays can enhance array resolution and DOA

\* Corresponding author.

E-mail address: [zhanghf@hit.edu.cn](mailto:zhanghf@hit.edu.cn) (H. Zhang).

estimation precision without increasing the array aperture, thereby confirming the superiority of vector signal processing. This article, along with related works on AVS (such as Kavoosi et al., 2021; Liang et al., 2023), adopts the vector signal processing framework proposed by Professor Arye Nehorai (Nehorai and Paldi, 1994). The milestone significance of the framework lies in the integration of vector sensors into traditional underwater acoustic signal processing. However, within this framework, the noise power of pressure and particle velocity outputs is unequal, resulting in array phase-amplitude errors. Additionally, due to the considerable complexity of noise fields in marine environments, correcting these phase-amplitude errors proves challenging in practical applications. Consequently, the significant inequality in array output noise poses substantial challenges to source count estimation and subspace partitioning, imposing limitations when dealing with low SNR data.

This paper introduces frequency-domain coherent processing techniques into vector array signal analysis to enhance DOA estimation performance under low SNR conditions. Coherent processing techniques, such as time-reversal deconvolution (Ma et al., 2017, 2018) and matched filtering (Yan, J. et al., 2022; Nnonyelu, C. J. et al., 2020; Kumar and Singh, 2023), effectively suppress random noise in observations while preserving coherent components. Due to their superior characteristics, coherent processing techniques find widespread application in active sonar detection and parameter estimation (Yang, T. C., 2017, 2018). The primary focus of this study is to leverage the characteristics of underwater acoustic vector measurement and apply coherent processing techniques to propose high-performance localization algorithms. Additionally, the study aims to delve into the mechanisms by which coherent processing enhances algorithm performance, and to assess the extent of its effects.

In underwater acoustic ambient noise, diffusive fields constitute the primary components. This type of noise demonstrates isotropic characteristics, marked by the absence of correlation between acoustic pressure and particle velocity (Barclay and Buckingham, 2013; Huang et al., 2012; Ren and Huang, 2020). Conversely, finite-scale acoustic sources exhibit a high degree of coherence between acoustic pressure and particle velocity. The coherence disparity between the oceanic noise field and underwater target sources forms the basis for the application of coherent processing.

The primary work of this paper is to leverage the frequency-domain coherent processing of acoustic pressure and particle velocity to construct array covariance matrices. Additionally, the paper introduces a multidimensional signal subspace method for DOA estimation by applying a focused transform.

The paper is organized as follows. In Section 2, we provide the problem formulation. In Section 3, the unbiasedness properties and asymptotic distribution of the proposed method are discussed. Section 4 analyzes the Cramér-Rao Bound (CRB) for wideband DOA estimation based on coherent processing. Section 5 validates the performance of the method through simulation, while Section 6 presents practical underwater acoustic environment tests to assess the applicability of the proposed approach.

## 2. Problem formulation

### 2.1. AVS array modeling and coherent processing

The main emphasis of this study lies in one-dimensional DOA estimation, with the exclusion of the Z-axis component of vibration velocity. If an array comprising  $m$  AVS, arranged equidistantly along a straight line with an inter-element spacing of  $L$ , is employed to capture signals from  $d$  far-field sound sources ( $d < m$ ), then the output of a single AVS can be expressed as:

$$\begin{bmatrix} p(t) \\ v_x(t) \\ v_y(t) \end{bmatrix} = \sum_{\xi=1}^d \begin{bmatrix} 1 \\ \cos \theta_\xi \\ \sin \theta_\xi \end{bmatrix} s_\xi(t - \tau_\xi) + \begin{bmatrix} n_p(t) \\ n_{v-x}(t) \\ n_{v-y}(t) \end{bmatrix} \quad (1)$$

Where. Explanation of parameters in Eq. (1).

$p(t)$	The output of the acoustic pressure channel in the AVS
$v_x(t)$ and $v_y(t)$	The outputs of the horizontal particle vibration velocities
$n_p(t)$ , $n_{v-x}(t)$ , $n_{v-y}(t)$	Gaussian white noise with isotropic properties
$s_\xi(t)$	The acoustic pressure complex envelope of the wave
$\Theta_0 = [\theta_1, \theta_2 \dots \theta_d]^T$	True DOA's
$m$	The number of array elements
$d$	The number of sources
$\tau_\xi = L \sin(\theta_\xi)/c$	Delay for the $\xi$ -th acoustic source is measured at the sensor with respect to the array reference point, $c$ is the speed of sound

Utilize matrix transformation to derive combination velocities exhibiting dipole-like directional characteristics that are mutually orthogonal.

$$\begin{bmatrix} v_c(t) \\ v_s(t) \end{bmatrix} = \begin{bmatrix} \cos \varphi & \sin \varphi \\ -\sin \varphi & \cos \varphi \end{bmatrix} \begin{bmatrix} v_x(t) \\ v_y(t) \end{bmatrix} \quad (2)$$

Where the symbol  $\varphi$  denotes the observation direction, which is occasionally referred to as the steering angle in certain literature.  $v_c(t)$  represents the projection of the particle velocity vector onto the observation direction, while  $v_s(t)$  signifies the projection of the particle velocity vector onto the direction perpendicular to the observation direction. In practical applications, if the approximate direction of the incoming waves is known, aligning  $\varphi$  with the direction of the incoming waves can lead to an increased SNR.

The array received data can be represented in the following format.

$$\begin{cases} \mathbf{p}(t) = [p_1(t), p_2(t) \dots p_m(t)]^T \\ = \mathbf{A}(\Theta_0) \mathbf{s}(t) + \mathbf{n}_p(t) \\ \mathbf{v}_c(t) = [v_{c-1}(t), v_{c-2}(t) \dots v_{c-m}(t)]^T \\ = \mathbf{A}(\Theta_0) \mathbf{\Phi} \mathbf{s}(t) + \mathbf{n}_{v-c}(t) \end{cases} \quad (3)$$

Assuming sufficiently extended duration of sensor output is observed. The sampled data is subsequently partitioned into  $N$  snapshots, each consisting of  $J$  samples. Within each snapshot, an FFT algorithm is applied to transform the data into the frequency domain. As a result,  $N$  sets of transformed data are obtained, with each set containing  $J$  frequency samples representing the spectrum of the observation vector. The array received data in the frequency domain can be represented in the following format.

$$\begin{cases} \mathbf{P}(f_i) = \mathbf{A}(f_i, \Theta_0) \mathbf{S}(f_i) + \mathbf{N}_p(f_i) \\ \mathbf{V}_c(f_i) = \mathbf{A}(f_i, \Theta_0) \mathbf{\Phi} \mathbf{S}(f_i) + \mathbf{N}_{v-c}(f_i) \end{cases} \quad i = 1, 2, \dots, J \quad (4)$$

Where. Explanation of parameters in Eq. (4).

$\mathbf{S}(f_i) = [S_1(f_i), \dots, S_d(f_i)]^T$	Acoustic source waveforms
$\mathbf{A}(f_i) = [\mathbf{a}(f_i, \theta_1), \dots, \mathbf{a}(f_i, \theta_d)]$	Array manifold
$\mathbf{a}(f_i, \theta_\xi) = [1, \exp(j 2\pi f_i \tau_\xi), \dots, \exp(j 2\pi f_i (m-1) \tau_\xi)]^T$	Steering vector
$\mathbf{\Phi} = \text{diag}[\cos(\varphi - \theta_1), \dots, \cos(\varphi - \theta_d)]$	Coefficient matrix for particle velocity
$\mathbf{N}_{v-c}(f_i) = \cos(\varphi) \mathbf{N}_{v-x}(f_i) + \sin(\varphi) \mathbf{N}_{v-y}(f_i)$	The projection of noise in the direction of $\varphi$

In the noise field, there is no correlation between acoustic pressure and particle velocity; hence, the following relationship prevails:

$$\begin{cases} \mathbb{E}[\mathbf{N}_p(f_i) \mathbf{N}_{v-x}^H(f_i)] = 0 \\ \mathbb{E}[\mathbf{N}_p(f_i) \mathbf{N}_{v-y}^H(f_i)] = 0 \end{cases} \quad (5)$$

where the superscript "H" represents the Hermitian transpose.

The pressure and particle velocity of far-field plane waves are coherent, establishing the basis for coherent processing. One specific form of coherent processing is as follows:

$$\mathbf{R}_i = \mathbf{P}(f_i) \mathbf{V}_c(f_i)^H \quad (6)$$

Substitute Eq. (4):

$$\mathbf{R}_i = \mathbf{A}(f_i, \theta_0) \mathbf{R}_s(f_i) \Phi \mathbf{A}(f_i, \theta_0)^H + \sigma_i^2 \mathbf{I} \quad (7)$$

Where

$$\mathbf{R}_s(f_i) = \mathbb{E}[\mathbf{S}(f_i) \mathbf{S}(f_i)^H]$$

$\mathbf{R}_i$  represents the correlation matrix at  $f_i$ , and  $\sigma_i^2$  represents the covariance between acoustic pressure and particle velocity in the noise field. If a sufficient number of snapshots are taken, that is, if there are enough measurement data bins at  $f_i$ , then  $\sigma_i^2$  tends toward 0, this forms the basis for coherent processing to suppress noise.

Considering that the array manifold  $\mathbf{A}(f_i, \theta_0)$  varies for different frequency bins, making it impractical to apply subspace methods, it becomes necessary to introduce a wideband focusing algorithm.

## 2.2. Two-sided correlation transformation for AVS wideband signal processing

The fundamental idea behind two-sided correlation transformation (TCT) is to perform focusing transformation on array-observed data, aligning the signal subspaces of wideband signal frequency components at a reference frequency, thereby mapping them into a unified signal subspace. The TCT focusing matrices are found by minimizing

$$\begin{aligned} & \min_{\mathbf{U}_i} \sum_{i=1}^J \left\| \mathbf{R}_0 - \mathbf{U}_i \mathbf{R}_i \mathbf{U}_i^H \right\|^2 \\ \text{s.t. } & \mathbf{U}_i^H \mathbf{U}_i = \mathbf{I}, i = 1, 2, \dots, J \end{aligned} \quad (8)$$

For the sake of simplicity, we will omit the frequency variable in the following discussions, representing  $\mathbf{A}(f_i, \theta_0)$  by  $\mathbf{A}_i$ ,  $\mathbf{U}(f_i)$  by  $\mathbf{U}_i$ , and so on.  $\mathbf{R}_0$  is the focusing noise-free correlation matrix. Eq. (8) is obtained as

$$\mathbf{U}_i = \mathbf{E}_0 \mathbf{E}_i^H \quad (9)$$

Where

$$\mathbf{R}_0 = \mathbf{E}_0 \bar{\Lambda}_0 \mathbf{E}_0^H, \mathbf{R}_i = \mathbf{E}_i \Lambda_i \mathbf{E}_i^H$$

Utilizing the focusing matrices  $\mathbf{U}_i$ , the observation vectors at different frequency bins undergo transformation into the focusing subspace. Specifically, new observation vectors are then constructed by

$$\begin{aligned} \mathbf{Q}(f_i) &= \mathbf{U}_i \cdot \mathbf{P}(f_i), i = 1, 2, \dots, J \\ \mathbf{Q}^V(f_i) &= \mathbf{U}_i \cdot \mathbf{V}_c(f_i), i = 1, 2, \dots, J \end{aligned} \quad (10)$$

These transformed observation vectors are employed to construct the sample correlation matrices.

$$\mathbf{R}_i^{(Q)} = \frac{1}{N} \sum_{n=1}^N \mathbf{Q}_n(f_i) \mathbf{Q}_n^V(f_i)^H \quad (11)$$

The universal focused sample correlation matrix, crucial for detection and estimation, is derived by averaging the aligned correlation matrices across frequency bins. This matrix is represented as

$$\mathbf{R}_0 = \frac{1}{J} \sum_{i=1}^J \mathbf{R}_i^{(Q)} = \frac{1}{J} \sum_{i=1}^J \mathbf{E}_0 \Lambda_i \mathbf{E}_0^H + \bar{\sigma}^2 \frac{1}{J} \sum_{i=1}^J \mathbf{U}_i \mathbf{U}_i^H \quad (12)$$

Where

$$\bar{\sigma}^2 = \frac{1}{J} \sum_{i=1}^J \sigma_i^2$$

As the number of snapshots approaches infinity,  $\bar{\sigma}^2$  tends to zero.  $\mathbf{R}$  can also be expressed as

$$\mathbf{R}_0 = \mathbf{E}_0 \bar{\Lambda}_0 \mathbf{E}_0^H \quad (13)$$

Where

$$\bar{\Lambda}_0 = \frac{1}{J} \sum_{i=1}^J \Lambda_i$$

Based on the preceding analysis, it becomes evident that the focusing transformation aligns distinct frequency components at a common frequency bin, thereby mapping them into a new subspace. This establishes the fundamental basis for the application of subspace methods. Concurrently, it ensures the method's unbiasedness, a topic that will be explored in subsequent sections. Conversely, the focusing error is a variable that changes with the focusing frequency bin, and an optimal focusing frequency bin exists to minimize this error. The latter part of this section will extensively explore the discussion on the optimal focusing frequency bin. It is crucial to note that the focusing frequency bin does not impact the algorithm unbiasedness.

Optimal  $f_i$  is determined through the following criteria:

$$\begin{aligned} \varepsilon &= \min_{f_0} \min_{\mathbf{U}_i} \sum_{i=1}^J \left\| \mathbf{R}_0 - \mathbf{U}_i \mathbf{R}_i \mathbf{U}_i^H \right\|^2 \\ \text{s.t. } & \mathbf{U}_i^H \mathbf{U}_i = \mathbf{I}, i = 1, 2, \dots, J \end{aligned} \quad (14)$$

In the practical computational procedure, the optimal focusing frequency can be determined through a one-dimensional search utilizing the following expression.

$$\min_{f_0} \sum_{\xi=1}^d \left| \sigma_\xi(\mathbf{R}_0) - \frac{\sum_{i=1}^J \sigma_\xi(\mathbf{R}_i)}{J} \right|^2 \quad (15)$$

## 2.3. The multidimensional signal subspace approach for DOA estimation

By leveraging the spatial relationship between the subspace of the correlation matrix  $\mathbf{R}_0$  and the array manifold  $\mathbf{A}_0$ , high-resolution localization of wideband sound sources is achieved. The Hermitian correlation matrix  $\mathbf{R}_0$  is subject to the following eigenvalue decomposition:

$$\mathbf{R}_0 = \mathbf{E}_0 \bar{\Lambda}_0 \mathbf{E}_0^H = \sum_{i=1}^m \lambda_i \mathbf{e}_i \mathbf{e}_i^H \quad (16)$$

Where:

$$\lambda_1 > \dots > \lambda_d > \lambda_{d+1} = \dots = \lambda_m = \bar{\sigma}^2$$

Partitioning the  $\mathbf{E}_0$  into the signal subspace  $\mathbf{E}_s$  and the noise subspace  $\mathbf{E}_n$ .

$$\mathbf{R}_0 = \mathbf{E}_s \Lambda_s \mathbf{E}_s^H + \mathbf{E}_n \Lambda_n \mathbf{E}_n^H \quad (17)$$

For a sufficiently snapshots,  $T \rightarrow \infty$ ,  $\bar{\sigma}^2 \rightarrow 0$ .

The  $\theta_0$  is obtained by maximizing the following criterion function.

$$\hat{\theta}_0 = \arg \max_{\theta} \mu(\theta) = \arg \max_{\theta} \text{tr}[\mathbf{P}_A(\theta) \mathbf{E}_s \mathbf{E}_s^H] \quad (18)$$

where  $\mathbf{P}_A$  is projection matrix, and  $\mathbf{P}_A = \mathbf{A}_0 \mathbf{A}_0^+ = \mathbf{A}_0 (\mathbf{A}_0^H \mathbf{A}_0)^{-1} \mathbf{A}_0^H$ .

#### 2.4. Wideband high-resolution DOA estimation algorithm for vector sensors

The algorithm is summarized as follows.

- (1) Apply FFT to the array output to sample the data spectrum. Divide the array into  $K$  data segments, each with  $N$  snapshots, and bandwidth-divide the signal in each segment into  $J$  parts.
- (2) Compute matrix  $\mathbf{R}_i$  according to Eq. (7).
- (3) Based on  $\mathbf{R}_i$ , obtain matrix  $\mathbf{R}_s(f_i)$  through matrix operations, and calculate the matrix  $\mathbf{R}_s(f_0) = \sum_{i=1}^J \mathbf{R}_s(f_i)$ .
- (4) Determine the focusing frequency and calculate matrix  $\mathbf{R}_0 = \mathbf{A}_0 \mathbf{R}_s(f_0) \mathbf{A}_0^H$ .
- (5) Identify the unitary transformation matrices using Eq. (9).
- (6) Multiply these matrices by the sample correlation matrices and average the results.
- (7) Conduct eigenvalue decomposition on the covariance matrix to extract the signal subspace and noise subspace.
- (8) Define the criterion functions. Based on the geometric relationship between the orthogonal basis of the subspace and the array manifold, a criterion function is established. For instance, the space formed by matrix  $\mathbf{A}_0$  is equivalent to the signal subspace. Projecting the signal subspace  $\mathbf{E}_s$  onto the array manifold across all angles in space, we define the 2-norm of this projection as the criterion function. The angle at which the evaluation function maximizes corresponds to the actual direction of arrival. This method is referred to as signal subspace fitting (SSF), as depicted in Eq. (18). Similar methodologies encompass noise subspace fitting (NSF), multiple signal classification (MUSIC), maximum likelihood estimation (ML), among others. Detailed descriptions can be found in the references (A. M. Elbir, 2020; X. Wang et al., 2022; Dar, Y. et al., 2020; Song, Y. et al., 2021; Langenbruch C, 2022).
- (9) Employing a multidimensional search approach to estimate the DOA. There are well-established multidimensional optimization algorithms available for seeking a set of angles that maximize the criterion function. In this study, genetic algorithms were employed. The principles and functionalities of optimization algorithms are documented in references (Shi Y et al., 2011; Sohail, 2023).
- (10) To improve the performance, iterate steps 2 to 9.

### 3. Performance analysis

#### 3.1. Unbiasedness analysis

The incorporation of coherent processing into vector array processing modifies the signal matrix, designated as  $\mathbf{R}'_s(f_i) = \mathbf{R}_s(f_i)\Phi$ . However, this alteration does not impact the array manifold  $\mathbf{A}_0$ ; the sample points continue to be confined within the previous plane. Consequently, both the signal subspace  $\mathbf{E}_s$  and the noise subspace  $\mathbf{E}_n$  remain unaffected. Thus, the introduction of coherent processing preserves the method unbiasedness.

DOA estimation depends on subspace methods and TCT. Of these, the subspace method is asymptotically unbiased. As the number of snapshots increases, the distortion of the subspace caused by noise decreases and approaches zero. Thus, both the subspace and DOA converge to their true values.

The unbiasedness of the TCT algorithm is elaborately described in reference (Valaee and Kabal, 1995). Its unbiasedness stems from the construction method of focusing matrix. Unlike CSS, which struggles to map and align the array manifold across various frequency points, leading to focusing errors, the TCT algorithm operates on the correlation matrix of each frequency point (as shown in Eq. (8)).

$$\mathbf{R}_0 = \frac{1}{J} \sum_{i=1}^J \mathbf{U}_i \mathbf{R}_i \mathbf{U}_i^H = \frac{1}{J} \sum_{i=1}^J \mathbf{E}_i \mathbf{A}_i \mathbf{E}_i^H = \mathbf{E}_0 \mathbf{A}_0 \mathbf{E}_0^H \quad (19)$$

As shown in Eq. (19), The transformation process does not induce any distortion in the subspace vectors, and the signal energy remains confined within the signal subspace without spreading into the noise subspace. Consequently, the proposed wideband DOA estimation algorithm in this paper is asymptotically unbiased.

#### 3.2. Asymptotic distribution

The TCT algorithm aligns various frequency components of the wideband signal within the same signal subspace, equating the DOA estimation to that of a single-frequency signal. Nevertheless, the focusing error exacerbates DOA estimation inaccuracies. For a single-frequency signal estimation, the normalized estimation error is asymptotically normal distributed with zero mean and covariance matrix  $\mathbf{C}$ . It is a function of noise power, where increased noise results in greater bias. Effectively controlling DOA bias involves suppressing noise components. In the context of a scalar sensors array, noise pertains to the variance of noise field acoustic pressure. Conversely, for a vector sensors array, noise is defined by the covariance between noise field acoustic pressure and particle velocity. Due to the lack of correlation between acoustic pressure and particle velocity in an isotropic noise field, the noise power of a vector sensors array is significantly smaller compared to that of a scalar sensors array. Consequently, the wideband DOA estimation method for the vector sensors array substantially improves DOA estimation performance.

### 4. The cramér-rao bound (CRB) for wideband DOA estimation

The introduction of vector signal coherent processing will impact the Cramér-Rao Bound (CRB) for parameter estimation. Specifically, in the context of wideband DOA estimation with a scalar pressure sensor array, the CRB traditionally depends on noise power. However, this paper introduces coherent processing techniques tailored for vector sensors, which replace noise power with the cross-covariance between acoustic pressure and particle velocity of the noise field. This alteration influences the CRB. The expression for the CRB for wideband DOA estimation in an AVS array is derived based on reference (D. N. Swigler, 1994), and it also needs to follow the assumptions regarding noise in this literature. Furthermore, precise alignment of the observation direction with the sound source is essential. While this expression elucidates the theoretical lower limit of DOA estimation, achieving such precision in practical applications may pose challenges.

Assuming the array acquires  $K$  data segments, each comprising  $N$  snapshots, and the signal in each data segment is bandwidth-divided into  $J$  parts, the expression for the CRB for wideband DOA estimation is given by

$$CRB(\theta_\xi) = \frac{p_N}{2KJp_\xi} [\mathbf{C}^{-1}]_{\xi\xi}, \xi = 1, 2, \dots, d \quad (20)$$

Where  $p_N$  represents the wideband noise power, and  $p_i$  is the power of the signal for the  $\xi$  th source.  $p_N = BW \sigma^2$ ,  $p_i = BW \mathbf{S}_\xi^H(f_i) \mathbf{S}_\xi(f_i)/N$ .

$$\mathbf{C} = \frac{1}{J} \sum_{i=1}^J \text{Re} \left[ \mathbf{D}^H \left( \mathbf{I} - \mathbf{A}_i (\mathbf{A}_i^H \mathbf{A}_i)^{-1} \mathbf{A}_i^H \right) \mathbf{D} \right]$$

$$\mathbf{D} = \left[ \frac{\partial \mathbf{a}(f_i, \theta_1)}{\partial \theta_1}, \frac{\partial \mathbf{a}(f_i, \theta_2)}{\partial \theta_2}, \dots, \frac{\partial \mathbf{a}(f_i, \theta_d)}{\partial \theta_d} \right]$$

### 5. Numerical examples and simulations

Examining the influence of coherent processing on DOA estimation performance using numerical examples. A scalar pressure sensor array

(SPSA) with identical parameters serves as a comparison. This section also analyzes the impact of key parameters such as SNR and the number of snapshots on the estimation results. The effectiveness of DOA estimation is quantified by the standard deviation of the estimated azimuth relative to the true direction.

We assume an eight-element Uniform Linear Array (ULA) with equal spacing between adjacent sensors, equivalent to half the wavelength at the center frequency. Two emitters of equal power are symmetrically located at  $8^\circ$  and  $-8^\circ$  with respect to the array broadside. In each case, signals from different acoustic sources are assumed to be uncorrelated. The output of each sensor is segmented into  $N$  snapshots, each consisting of 8 samples. Subsequently, an FFT algorithm is applied to sample the spectrum of the observations, considering a 100% relative bandwidth. We conduct 300 independent trials and calculate the deviation of the first DOA estimate. The specific simulation parameters are shown in the Table 1.

The first example is chosen to illustrate the necessary number of snapshots, with the signal having a power level 10 dB above the noise. And the standard deviation of DOA estimations is depicted in Fig. 1. CP-AVS stands for coherent processing using an acoustic vector sensor array, represents the method proposed in this paper, while SPSA represents the result from a scalar pressure sensor array.

In this illustrative case, the standard deviations across various algorithms consistently decrease as the number of snapshots increases. Notably, the AVS array wideband DOA estimation method demonstrates similar standard deviation values compared to SPSA method, yet it exhibits reduced standard deviations, indicating an improved performance in DOA estimation.

The second example is chosen to illustrate depict the impact of SNR on DOA estimation performance. The output of each sensor is segmented into 64 snapshots, each consisting of 8 samples. The specific simulation parameters are shown in the Table 2. And the standard deviation of DOA estimations is depicted in Fig. 2.

The AVS array wideband DOA estimation method exhibits superior performance, evidenced by a smaller standard deviation closer to the CRB when compared to the SPSA method, especially in low SNR scenarios. A comprehensive analysis of the asymptotic distribution reveals that noise power plays a pivotal role in influencing the accuracy of DOA estimation.

The preceding analysis has only illustrated the advantages of coherent processing methods for vector arrays over scalar arrays. To comprehensively evaluate the performance of the proposed method, it is essential to introduce other methods for comparison. Consider the following three scenarios.

Incoherent processing using an acoustic vector sensor array (Abbreviation as IP-AVS.): the pressure and particle velocity data are not subjected to coherent processing. The particle velocity data remains relatively independent, akin to the addition of directional sensors. This modeling approach is cited from the literature (Chen and Zhao, 2005).

**CP-AVS:** A vector array method that utilizes coherent processing between acoustic pressure and particle velocity to achieve noise reduction, as well as SPSA. These two methods have been used in the previous two examples.

The approach outlined in this paper employs subspace methods to

**Table 1**  
Parameters set in the first numerical examples.

Parameter	Value
The number of emitters	2
The number of sensors in the linear array	8
True DOAs	$-8^\circ$ $8^\circ$
Signal snapshots	8~8192
SNR	10 dB
Band wide	100% relative bandwidth
Number of frequency bins	8
trials	300

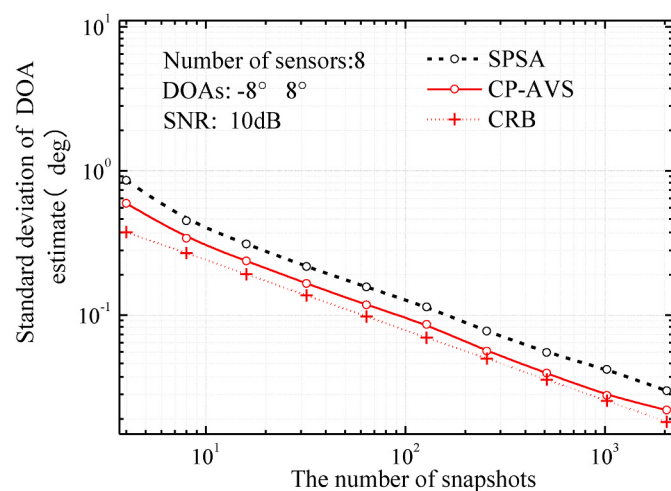


**Fig. 1.** Standard deviation of DOA estimations relative to the number of snapshots.

**Table 2**  
Parameters set in the second numerical examples.

Parameter	Value
The number of emitters	2
The number of sensors in the linear array	8
True DOAs	$-8^\circ$ and $8^\circ$
Signal snapshots	64
SNR	$-10\text{--}20$ dB
Band wide	100% relative bandwidth
Number of frequency bins	8
trials	300

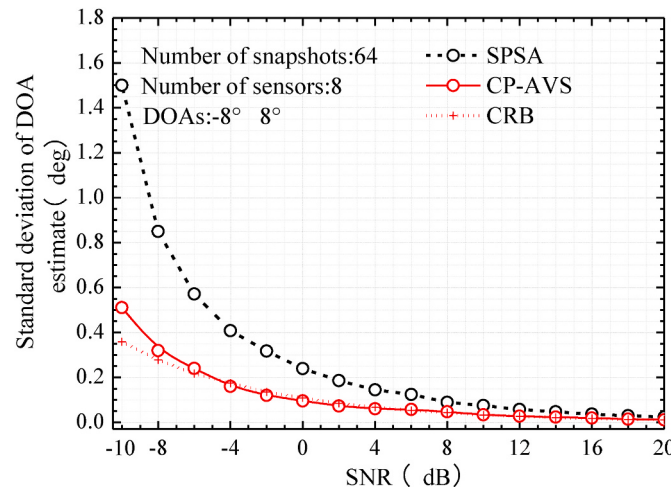


**Fig. 2.** Standard deviation of DOA estimations relative to SNR.

convert azimuth estimation into a multidimensional search problem. It is understood that different subspace methods will inherently yield diverse effects on the estimation outcomes. While SSF was initially used, subsequent examples explore alternative methods like NSF and MUSIC. This demonstrates the adaptability of coherent processing applications.

The standard deviations of DOA estimation are provided in the following table. With a SNR of 10 dB and 64 snapshots, all other parameters remain consistent with the previous settings. The analysis results are presented in Table 3.

Coherent processing with an AVS array significantly enhances source localization accuracy, as evident from the markedly reduced standard

**Table 3**

Standard deviation of DOA estimations(deg).

Types of subspace methods	SPSA	IP-AVS	CP-AVS
SSF	0.074	0.069	0.034
NSF	0.077	0.063	0.041
MUSIC	0.089	0.079	0.047
ML	0.071	0.065	0.030
CRB	0.070	—	0.022

deviation associated with this method. In the case of IP-AVS, it is comparable to expanding the array element count, leading to only a modest improvement in algorithm performance. Coherent processing technique, not only mitigates bias in DOA estimation but also diminishes the CRB.

## 6. Experimental Validation and analysis

The absence of correlation between acoustic pressure and particle velocity in the noise field is a critical factor in enhancing the performance of the proposed method. In simulated analyses, assuming isotropic Gaussian white noise satisfies this criterion. In practical underwater acoustic environments, various noise sources, including distant ship operations, biological sounds, as well as wind and rain noise, coexist. While these noises aren't entirely isotropic, there is a noticeable level of correlation between acoustic pressure and particle velocity in the underwater noise field. Consequently, validating the applicability of the proposed method in real-world underwater acoustic environments becomes imperative.

The MEMS AVS utilized in this experiment comprises a MEMS chip (see Fig. 3), a piezoelectric ceramic ring, and a polyurethane housing. It includes three signal outputs: X, Y, and P, which can synchronously detect the vector information and scalar information of the acoustic field particles. Among them, the X and Y channels are velocity output channels, while the P channel is a scalar pressure output channel.

This experiment utilized underwater explosive events to generate wideband shock signals. A receiving array was deployed approximately 100 m from the explosion point, consisting of a three-element vector sensor array with an inter-element spacing of 0.375 m. The system operated with a sampling frequency of 10 kHz. Power spectral analysis was performed on 1-s acoustic pressure measurement data post-explosion and background noise test data. The results are depicted in the Fig. 4.

From Fig. 4, it is evident that the energy of the wideband signal generated by the explosion is predominantly concentrated in the mid to low-frequency range. The power spectral density exhibits an increasing then decreasing trend, reaching its peak around 400 Hz. In the background noise, there is a disturbance at approximately 1 kHz. This is caused by the equipment on the test boat, and its amplitude is approximately 10 dB lower than that of the explosion sound, therefore it is

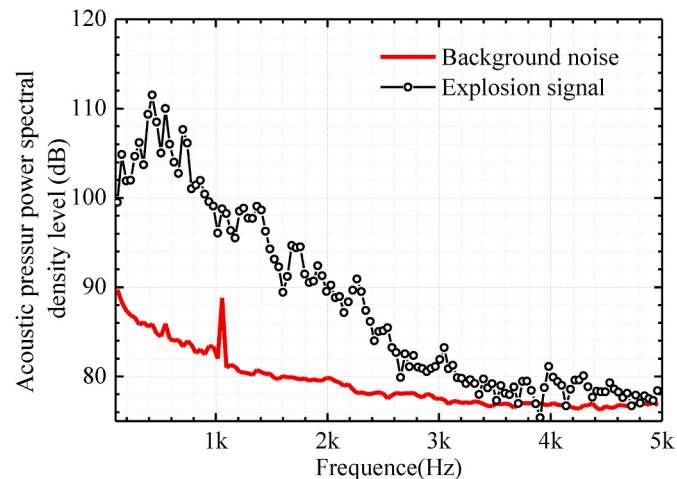


Fig. 4. The acoustic pressure power spectral density level of blast-induced wideband shock signals and background noise.

believed that it will not significantly affect the test results.

The frequency-domain correlation between acoustic pressure and particle velocity at any point in the sound field is denoted by the following function. Its significance is rooted in the square of the normalized sound intensity within the sound field at a specific frequency.

$$\gamma_{p,v-x}^2(f_i) = \frac{|R(f_i)|^2}{P(f_i)^2 V_x(f_i)^2}, 0 \leq \gamma_{p,v-x}^2(f_i) \leq 1$$

$$\gamma_{p,v-y}^2(f_i) = \frac{|R(f_i)|^2}{P(f_i)^2 V_y(f_i)^2}, 0 \leq \gamma_{p,v-y}^2(f_i) \leq 1 \quad (21)$$

The coherence functions were computed, and the results are visually presented in the Fig. 5 and 6.

Upon analyzing the above figure, it is evident that the wideband shock signal generated by the explosion is predominantly focused in the frequency range below 3 kHz, demonstrating robust correlation within this frequency interval. Conversely, the coherence function of background noise exhibits a gradually increasing trend across the entire frequency spectrum, with relatively smaller values in the low-frequency range.

The coherence function of the background noise continues to show a peak around 1 kHz, signifying the persistence of coherent interference. Nevertheless, given the interference constrained amplitude and narrow bandwidth, its impact on the results is deemed minimal.

Utilizing the method outlined in Section 5 for wideband DOA estimation, an FFT window length of 512 is employed. The coherent matrix

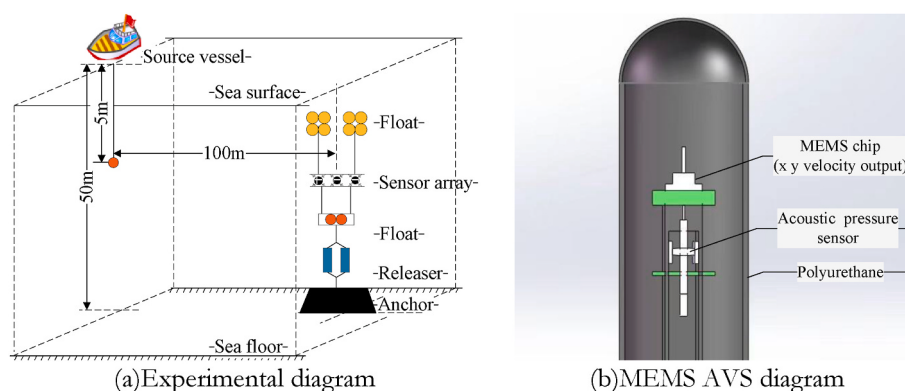
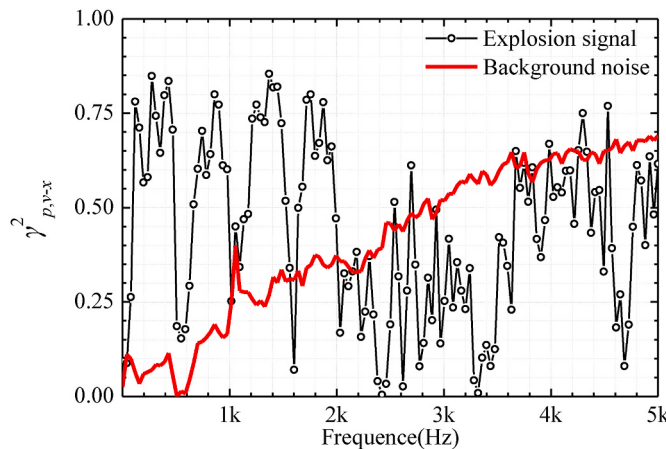
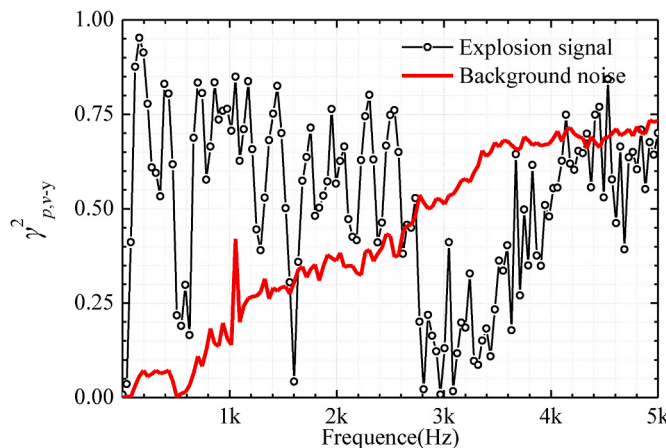


Fig. 3. Experimental and AVS diagram.



**Fig. 5.** Coherence functions of acoustic pressure and particle velocity for explosive signals and background noise in the horizontal x direction.



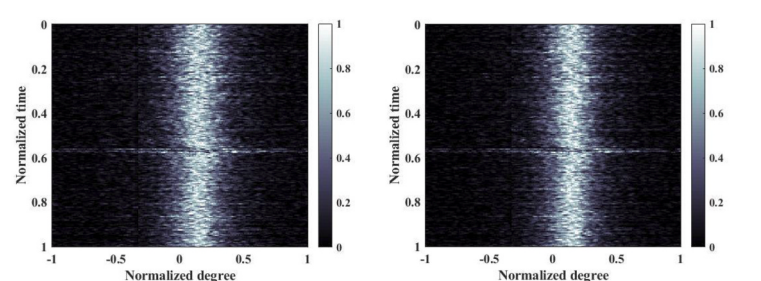
**Fig. 6.** Coherence functions of acoustic pressure and particle velocity for explosive signals and background noise in the horizontal y direction.

estimation is then conducted with a focus on these frequency components. Following this, high-resolution DOA estimation is achieved through the subspace method. To provide a baseline, the SPSA and IP-AVS are employed as comparison. The results are detailed in Fig. 7.

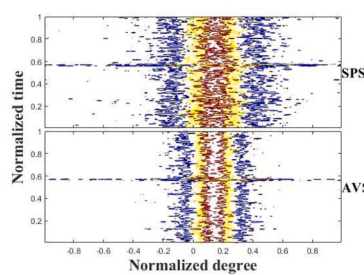
Based on the Fig. 7, it is evident that the spatial spectrum distribution achieved by the CP-AVS wideband DOA estimation method is more concentrated, leading to superior performance in DOA estimation. Consequently, despite the correlation between acoustic pressure and particle velocity in the actual underwater acoustic environment noise field, the coherent processing employed by the acoustic vector sensor effectively mitigates noise components in the array-received data. As a result, the wideband DOA estimation using CP-AVS achieves enhanced DOA estimation performance.

## 7. Conclusion

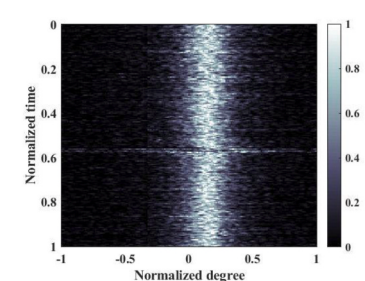
In this paper, we have introduced a method for localization of broadband signals using an AVS array. The motivation behind this work was to mitigate isotropic background noise by utilizing the coherent processing between acoustic pressure and particle velocity, aiming to minimize the error in DOA estimation. The normalized estimation error is a function of noise power, where, for vector coherent processing, its equivalent noise power is represented by the covariance between the acoustic pressure and particle velocity in the noise field. The diminished correlation between the acoustic pressure and particle velocity in an isotropic noise field substantially diminishes both the estimation error and the CRB for wideband DOA estimation when employing coherent processing. Adapting to the challenge of inconsistent array manifolds across different frequencies in wideband signals, the TCT algorithm is introduced. This algorithm effectively maps various frequency components to the same signal subspace, producing an output that serves as a highly accurate approximation of the focused subspace. By incorporating a multidimensional subspace method, this approach ensures an asymptotically unbiased estimation for source localization. In the simulation and experimental studies, the proposed method exhibits superior performance in DOA estimation, displaying a smaller estimation error that closely approaches the CRB. Furthermore, it demonstrates excellent adaptability in practical underwater acoustic experiments.



(a) The spatial spectrum of SPSA



(c) Contour plots of SPSA and CP-AVS spatial spectrum (d) The spatial spectrum of CP-AVS



(b) The spatial spectrum of IP-AVS

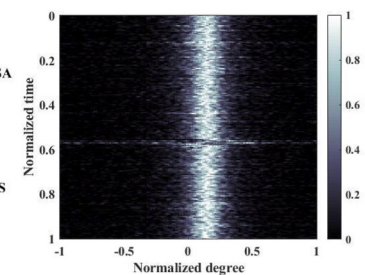


**Fig. 7.** Result of DOA estimations.

## CRediT authorship contribution statement

**Bowen Dong:** Visualization, Validation, Software, Methodology, Investigation, Formal analysis, Data curation, Conceptualization, Writing – original draft, Writing – review & editing. **Haifeng Zhang:** Conceptualization, Data curation, Project administration, Resources, Supervision. **Shengtian Sang:** Investigation, Resources, Software, Supervision. **Yan Zhang:** Validation, Visualization, Writing – review & editing.

## Declaration of competing interest

The authors declare that they have no known competing financial interests or personal relationships that could have appeared to influence the work reported in this paper.

## Data availability

Data will be made available on request.

## Acknowledgement

This work was supported by the National Key R&D Program of China (Grant No. 2022YFB3205403).

## Appendix A. Supplementary data

Supplementary data to this article can be found online at <https://doi.org/10.1016/j.oceaneng.2024.117882>.

## References

- Abraham, D.A., 2019. Underwater Acoustic Signal Processing: Modeling, Detection, and Estimation. Springer, Cham, Switzerland, pp. 356–358.
- Chen, J.C., Yip, L., Elson, J., Wang, H., Maniezzo, D., Hudson, R.E., et al., 2003. Coherent acoustic array processing and localization on wireless sensor networks. Proc. IEEE 91 (8), 1154–1162.
- Jiang, M., Nnonyelu, C.J., Lundgren, J., Thungström, G., Sjöström, M.A., 2023. Coherent wideband acoustic source localization using a Uniform circular array. Sensors 23 (11), 5061. <https://doi.org/10.3390/s23115061>.
- Wang, H., Kaveh, M., 1985. Coherent signal-subspace processing for the detection and estimation of angles of arrival of multiple wideband sources. IEEE Trans. Acoust. Speech Signal Process. 33 (4), 823–831.
- Valaee, S., Kabal, P., 1995. Wide-band array-processing using a 2-sided correlation transformation. IEEE Trans. Signal Process. 43 (1), 160–172.
- Chen, Huawei, Zhao, Junwei, 2005. Coherent signal-subspace processing of acoustic vector sensor array for DOA estimation of wideband sources. Signal Process. 85 (4), 837–847. <https://doi.org/10.1016/j.sigpro.2004.07.030>.
- Kavoosi, V., Dehghani, M.J., Javidan, R., 2021. Underwater acoustic source positioning by isotropic and vector hydrophone combination. J. Sound Vib. 501.
- Liang, Y., Chen, Y., Meng, Z., Lu, Y., Wang, J., Ma, S., Hu, X., Li, W., Zhang, Y., 2023. Research on the broadband source localization of a vector hydrophone vertical line array in the deep sea. Ocean Eng. 280.
- Nehorai, A., Paldi, E., 1994. Acoustic vector-sensor array-processing. IEEE Trans. Signal Process. 42, 2481–2491.
- Ma, L., Zhao, A., Hui, J., Zeng, C., Bi, X., 2017. An improved target detection and azimuth angle estimation method using a single acoustic vector sensor. J. Acoust. Soc. Am. 142 (4), 2587.
- Ma, L., Zhao, A., Aaron Gulliver, T., Zeng, C., 2018. Experimental performance evaluation of underwater active detection and positioning system. J. Acoust. Soc. Am. 144 (3), 1770.
- Yan, J., Avagyan, M., Colgan, R.E., Veske, D., Bartos, I., Wright, J., Márka, S., 2022. Generalized approach to matched filtering using neural networks. Phys. Rev. D 105 (4), 043006.
- Nnonyelu, C.J., Wong, K.T., Lee, C.H., 2020. Higher-order figure- 8 sensors in a pair, skewed and collocated—their azimuthal “spatial matched filter” beam-pattern. J. Acoust. Soc. Am. 147 (2), 1195–1206.
- Kumar, K.S., Singh, N.P., 2023. Segmentation of retinal blood vessel using generalized extreme value probability distribution function (pdf)-based matched filter approach. Pattern Anal. Appl. 26 (1), 307–332.
- Yang, T.C., 2017. Deconvolved conventional beamforming for a horizontal line array. IEEE J. Ocean. Eng. 43 (1), 160–172.
- Yang, T.C., 2018. Performance analysis of superdirective circular arrays and implications for sonar systems. IEEE J. Ocean. Eng. 44 (1), 156–166.
- Barclay, D.R., Buckingham, M.J., 2013. Depth dependence of wind-driven, broadband ambient noise in the Philippine Sea. J. Acoust. Soc. Am. 133 (1), 62–71.
- Ren, C., Huang, Y., 2020. A spatial correlation model for broadband surface noise. J. Acoust. Soc. Am. 147 (2), EL99.
- Huang, Y., Ren, Q., Li, T., 2012. A geometric model for the spatial correlation of an acoustic vector field in surface-generated noise. J. Mar. Sci. Appl. 11 (1), 119–125.
- Elbir, A.M., 2020. DeepMUSIC: multiple signal classification via deep learning. IEEE Sensors Letters 4 (4), 1–4. <https://doi.org/10.1109/LSENS.2020.2980384>.
- Wang, X., Yang, L.T., Meng, D., Dong, M., Ota, K., Wang, H., 2022. Multi-UAV cooperative localization for marine targets based on weighted subspace fitting in SAGIN environment. IEEE Internet Things J. 9 (8), 5708–5718. <https://doi.org/10.1109/JIOT.2021.3066504>.
- Dar, Y., Mayer, P., Luzi, L., Baraniuk, R., 2020. Subspace fitting meets regression: the effects of supervision and orthonormality constraints on double descent of generalization errors. In: Proceedings of the 37th International Conference on Machine Learning, in Proceedings of Machine Learning Research119, pp. 2366–2375.
- Song, Y., Durkan, C., Murray, I., Ermon, S., 2021. Maximum likelihood training of score-based diffusion models. Adv. Neural Inf. Process. Syst. 34, 1415–1428.
- Langenbruch, C., 2022. Parameter uncertainties in weighted unbinned maximum likelihood fits. The European Physical Journal C 82 (5), 393.
- Shi, Y., Tian, Y., Kou, G., Peng, Y., Li, J., 2011. Optimization Based Data Mining: Theory and Applications. Springer, Berlin.
- Sohail, A., 2023. Genetic algorithms in the fields of artificial intelligence and data sciences. Ann. Data. Sci. 10, 1007–1018. <https://doi.org/10.1007/s40745-021-00354-9>.
- Swingler, D.N., 1994. An approximate expression for the cramer-rao Bound on DOA estimation of closely spaced sources in broadband line-array beamforming. IEEE T-SP 42 (No.6), 1540–1543.